Membrane-Free Battery for Harvesting Low-Grade Thermal Energy

Citation: Yang, Yuan, James Loomis, Hadi Ghasemi, Seok Woo Lee, Yi Jenny Wang, Yi Cui, and Gang Chen. "Membrane-Free Battery for Harvesting Low-Grade Thermal Energy." Nano Lett. 14, no. 11 (November 12, 2014): 6578–6583.

As Published: http://dx.doi.org/10.1021/nl5032106

Publisher: American Chemical Society (ACS)

Persistent URL: http://hdl.handle.net/1721.1/99726

Version: Author's final manuscript: final author's manuscript post peer review, without publisher's formatting or copy editing

A Membrane-free Battery for Harvesting Low-grade Thermal Energy

Yuan Yang[1], James Loomis[1], Hadi Ghasemi[1], Seok Woo Lee[2], Jenny Wang[1], Yi Cui[2,3a] and Gang Chen[1a]

[1]*Department of Mechanical Engineering, Massachusetts Institute of Technology, Cambridge, MA, 02139, USA.* [2]*Department of Materials Science and Engineering, Stanford University, Stanford, CA, 94305, USA.* [3]*Stanford Institute for Materials and Energy Sciences, SLAC National Accelerator Laboratory, 2575 Sand Hill Road, Menlo Park, CA 94025, USA.*

[a]To whom correspondence should be addressed. Email: gchen2@mit.edu yicui@stanford.edu

Abstract

Efficient and low-cost systems are desired to harvest the tremendous amount of energy stored in low-grade heat sources (< 100 ℃). An attractive approach is the thermally regenerative electrochemical cycle (TREC), which uses the dependence of electrode potential on temperature to construct a thermodynamic cycle for direct heat-to-electricity conversion. By varying the temperature, an electrochemical cell is charged at a lower voltage than discharged; thus, thermal energy is converted to electricity. Recently a Prussian blue-based system with high efficiency has been demonstrated. However, the use of an ion-selective membrane in this system raises concerns about the overall cost,

which is crucial for waste heat harvesting. Here we report on a new membrane-free battery with a nickel hexacynoferrate (NiHCF) cathode and a silver/silver chloride anode. The system has a temperature coefficient of -0.74 mV K^{-1}. When the battery is discharged at 15 ^{o}C and recharged at 55 ^{o}C, a thermal-to-electricity conversion efficiency of 2.6% and 3.5% is achieved with assumed heat recuperation of 50% and 70%. This work opens new opportunities for using membrane-free electrochemical systems to harvest waste heat.

A vast amount of low-grade heat (<100 ^{o}C) exists in industrial processes, the environment, biological entities, solar-thermal and geothermal energy.[1-3] Conversion of this low-grade heat to electricity is difficult due to the distributed nature of these heat sources and the low temperature differential. Different technologies, such as solid-state thermoelectric energy conversion[4-7] and organic Rankine cycles[1, 8], are being actively investigated but face their own challenges in energy conversion efficiency, cost, and system complexity. Thermally regenerative electrochemical cycle (TREC) is an alternative approach based on the temperature dependence of cell voltage of electrochemical systems.[9-12] For a full cell reaction A+B → C+D (discharge), the temperature coefficient α is defined as

$$\alpha = \frac{\partial E}{\partial T} = -\frac{1}{nF}\frac{\partial \Delta G}{\partial T} = \frac{\Delta S}{nF} \qquad (1)$$

where E is the full cell voltage, T is the temperature, n is the number of electrons transferred in the reaction, F is Faraday's constant. ΔG and ΔS are the change of partial molar Gibbs free energy and partial molar entropy in the full cell reaction.[12-14] If α is negative, net electricity can be produced by discharging the cell at low temperature (T_L)

and recharging at high temperature (T_H) with lower voltage (Figure 1a). If α is positive, electricity is produced by discharging at T_H and recharging at T_L. In both cases, the work generated originates from heat absorbed at T_H, indicated as entropy increase in the temperature-entropy (T-S) diagram (Figure 1b). The T-S diagram clearly shows that TREC is an Ericsson cycle with isothermal charge/discharge processes and isobaric heating/cooling processes. The corresponding heat-to-electricity conversion efficiency (η) of TREC can be expressed as

$$\eta = \frac{W}{Q_H + Q_{HR}} = \frac{\Delta S \Delta T - E_{loss}}{T_H \Delta S + (1 - \eta_{HR}) C_p \Delta T} \qquad (2)$$

where W is the difference between discharge and charge energy in a cycle. Q_H is the heat absorbed at T_H. Q_{HR} is the extra energy needed to heat the cell up. E_{loss} is the energy loss due to internal resistance of the cell. ΔS is the entropy change in reaction. $\Delta T = T_H - T_L$. C_p is the heat capacity of the cell. η_{HR} is the heat recuperation efficiency, indicating how much energy rejected in the cooling process can be used for the heating process. Theoretically η_{HR} can reach 100%, and 50-70% has been proven to be reasonable with experiments[9]. From equation (2), the theoretical efficiency of TREC is the Carnot limit while practical efficiency is mainly limited by the heat capacity of materials, the heat recuperation efficiency[15] and the internal resistance of the cell. This is in contrary to thermoelectric devices which are mainly limited by transport properties of phonons and electrons.

The concept of TREC was developed a few decades ago and focused on high temperature applications (500 - 1500 ℃) and showed efficiencies up to 40-50% of the Carnot limit. However, low temperature TREC did not received as much attention since

electrode materials with low polarization and high charge capacity at low temperature were limited[16]. There was no data presented on charge/discharge voltage profiles and efficiencies. Recently, a new thermally regenerative electrochemical cycle (TREC) based on a copper hexacyanoferrate (CuHCF) cathode and a Cu/Cu^{2+} anode was demonstrated for harvesting low-grade heat.[9] The low polarization of electrodes, moderate temperature coefficient, high charge capacity and low heat capacity led to a high efficiency. An efficiency of 5.7% was demonstrated when the cell was operated between 10 and 60 ^{o}C assuming a heat recuperation efficiency of 50%.[9]

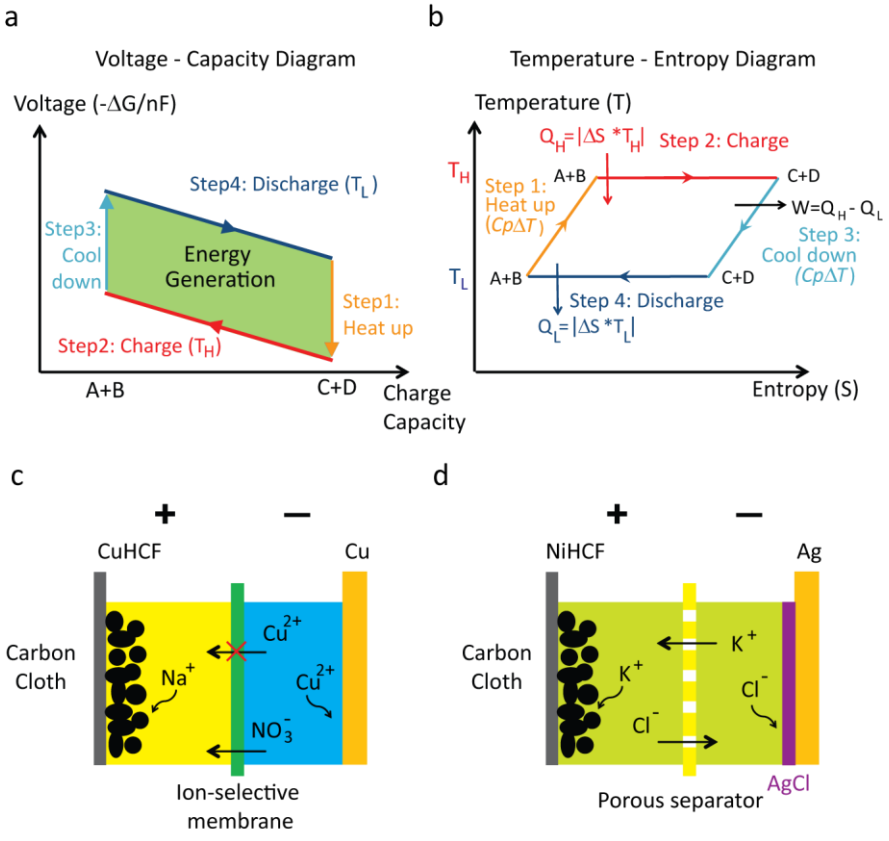

Figure 1. Schematic of thermally regenerative electrochemical cycle (TREC). a) The voltage-capacity plot of a TREC. Net energy is generated since the discharge voltage is higher than charge voltage. The case with negative α is presented. b) The corresponding temperature-entropy

(T-S) plot. c) A TREC with an ion-selective membrane to block certain ions to avoid side reactions. d) The membrane-free NiHCF/Ag/AgCl system with no unwanted reaction between electrodes and ions.

One potential issue of the CuHCF//Cu^{2+}/Cu system is the use of ion-selective membrane to allow NO_3^- anion passing through but not Cu^{2+} cations to avoid side reaction between CuHCF and Cu^{2+} (Figure 1c). Ion-selective membranes are currently expensive and difficult to completely block penetration of Cu^{2+} in long-term operation. Finding membrane-free systems to lower the cost and facilitate long-term operation would make TREC systems more ideal. To address this issue, we apply a criterion that any soluble chemical species in electrolyte should not induce adverse side reactions other than the desired two half-cell reactions. In this paper, a membraneless electrochemical system with a nickel hexacyanoferrate (NiHCF, $KNi^{II}Fe^{III}(CN)_6$) cathode and a silver/silver chloride anode is demonstrated, where no adverse side reaction is introduced due to solutes in electrolyte (Figure 1d) . The reactions of the two half cells are:

$$\text{Cathode: } KNi^{II}Fe^{III}(CN)_6 + K^+ + e^- \rightarrow K_2Ni^{II}Fe^{II}(CN)_6$$

$$\text{Anode: } AgCl + e^- \rightarrow Ag + Cl^-$$

In this system, ions involved in each electrode do not have side reactions with each other, so the ion-selective membrane is unnecessary and can be replaced by an inexpensive porous separator. The full cell has a temperature coefficient of -0.74 ± 0.05 mV K^{-1} and a thermal-to-electricity conversion efficiency of 2.6% and 3.5% when cycled between 15 and 55 ^oC with assumed heat recuperation efficiency of 50% and 70%, respectively.

NiHCF nanoparticles were synthesized using a simple solution approach by dropping 50 mM $Ni(NO_3)_2$ aqueous solution into 25 mM $K_3Fe(CN)_6$ aqueous solution at

$50^{o}C$[17, 18]. The average size of as-synthesized particles is ~50 nm (Figure S1). The small particle size enhances surface area for reaction and reduces distance for ionic transport in solid, leading to fast kinetics and lower overpotential. The porous Ag/AgCl electrode was made by charging Ag film in KCl aqueous solution. Ag/AgCl has an oxidation/reduction voltage gap due to a combination of considerable nucleation barrier and AgCl self-resistance[19]. This issue is tackled by using porous electrode with high surface area. The electrolyte was 3 M KCl with 0.2 M $Ni(NO_3)_2$ aqueous solution. Ni^{2+} was used to stabilize NiHCF at high temperature based on the common ion effect[20]. The pH of the electrolyte was tuned to 2 by HNO_3 to optimize the performance of NiHCF[17]. A silver wire with pre-oxidized AgCl was used as the reference electrode. Glassfiber filter was used as the separator to prevent battery shorting. The NiHCF and AgCl electrodes were assembled in a pouch cell configuration (Figure S2). Details on electrode preparation and assembly of the pouch cell are described in the supporting information.

Temperature-dependent electrochemical characteristics were measured with a home-made temperature cycler (Figure 2a and Figure S3). The thin pouch cell was sandwiched between two thermoelectric plates and thermocouples were attached to the surface of the pouch cell. Thermal paste was applied to all interfaces to ensure good thermal contact. Temperatures of thermocouples were acquired by a data acquisition (DAQ) board and controlled with fluctuations less than 0.1 ^{o}C. This compact design allows the temperature to be switched in less than three minutes so that other effects, such as self-discharge and dissolved oxygen, can be minimized. An example of measuring electrode voltage at different temperatures is shown in Figure S4. Each temperature step lasted for eight minutes and the voltage became steady after three minute in each step,

indicating that the system quickly reached equilibrium and there was no obvious effect due to self-discharge.

The effect of temperature on the full cell voltage is investigated first (Figure 2b – d). Figure 2b shows the dependence of full cell voltage on temperature at different states of charge (SOC) for the 3 M KCl cell. The number on the right side is in the unit of mAh g^{-1}. 0 mAh g^{-1} is the fully discharged state. For all measurements, the full cell voltage is linearly related to the temperature in the range of 15 to 55 ^{o}C, indicating that α is a constant in the temperature range. α of the full cell at different SOC with [KCl] from 1 to 4 M are presented in Figure 2c. For all concentrations, α shows an inverse bell shape against SOC. α is flat in the middle of the voltage curve (10-50 mAh g^{-1}), but its absolute value becomes smaller when the system approaches a fully charged or a fully discharged state. Moreover, lower [KCl] always leads to a more negative temperature coefficient for all SOC, which is likely a result of changes in K^+ and Cl^- activity. For instance, plot of α at 50% SOC against [KCl] shows a trend consistent with the derivation of α from Nernst equation (Figure 2c):

$$E = E_0 + \frac{RT}{F}\ln([K^+][Cl^-]) \qquad (3a)$$

$$\alpha = \alpha_0 + \frac{R}{F}\ln([K^+][Cl^-]) = \alpha_0 + 0.0862\text{mV } K^{-1}\ln([K^+][Cl^-]) \qquad (3b)$$

where E is the electrode potential, R is the ideal gas constant, and F is the Faraday constant (96485 C mol^{-1}). E_0 and α_0 are the electrode potential and temperature coefficient with unit activity of ions for a certain SOC. The activities of solid phases are assumed to be 1 so they are not shown in the equation. The activity coefficients of ions

are assumed to be 1 so that activities of ions are replaced by concentration. The deviation from Nernst equation may arise from the activity coefficient and influence of Ni^{2+}, which can also be inserted into NiHCF[20]. The temperature coefficient mainly comes from the half cell of NiHCF, as previous studies show that the temperature coefficient of Ag/AgCl is 0.22-0.26 mV K^{-1} with 1 M KCl[12] and 0.12 mV K^{-1} with 4 M KCl[9]. The measured temperature coefficient is slightly more negative than CuHCF[9], which is the reason why we use NiHCF instead of CuHCF. In our measurement, although the reference electrode and anode are the same, a small difference in electrode potential is observed (~0.04 mV/K). The origin is unclear and may be related to the preparation process of reference electrode, which exposed the electrode in air and light and may result in difference in chemical composition. In order not to overestimate α and energy conversion efficiency, α of the full cell is calculated based on the potential of NiHCF cathode and Ag/AgCl anode and its absolute value is less than that between the cathode and the reference electrode.

The dependence of α on [KCl] leads to a trade-off between voltage gap ($|\alpha\Delta T|$) and heat capacity. Since K^+ and Cl^- are stored in the electrolyte, higher [KCl] indicates a smaller amount of KCl electrolyte is required and thus less energy is needed to heat the system up. However, it also reduces the absolute value of α and the voltage gap between discharge and charge ($|\alpha\Delta T|$). After estimating the conversion efficiency at different concentrations, 3 M was chosen as the optimal concentration and used in following tests (Table S1).

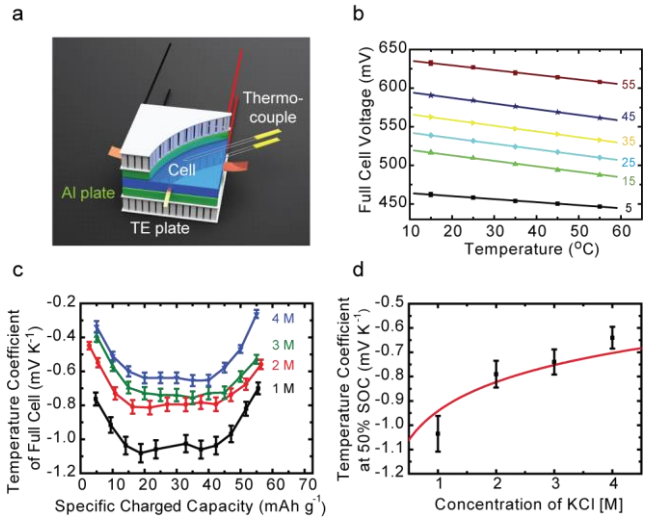

Figure 2. Temperature coefficient of the NiHCF/Ag/AgCl system. a) A schematic of the experimental setup for measuring temperature coefficient. b) The temperature-dependent voltage of a full cell at different states of charge (SOC). The number on the right indicates capacity charged in the unit of mAh g^{-1}. 0 mAh g^{-1} refers to the fully discharged state. The electrolyte is 3 M KCl. c) The temperature coefficient at different SOC and concentrations of KCl electrolyte. d) The dependence of temperature coefficient on the concentration of KCl solution at 50% SOC. The red curve is fitting based on equation (3). For all measurements, 0.2 M $Ni(NO_3)_2$ was added to stabilized NiHCF and HNO_3 was used to tune the pH of the solution to 2.

Figure 3a shows the thermal cycle of a NiHCF/Ag/AgCl full cell with 3M KCl/0.2 $Ni(NO_3)_2$ electrolyte. The temperature is well controlled with a fluctuation less than 0.1 ^oC. At the end of each discharge or charge, the cell was rested for three minutes to allow the temperature to change and the system to reach equilibrium. Voltage vs. capacity at currents of 1 C (40 mA g^{-1}) and C/2 (20 mA g^{-1}) are presented as Figure 3b and 3c, respectively. All electrode potentials discussed below are versus Ag/AgCl reference electrode exposed to the same electrolyte in the pouch cell. The current rate and specific capacity are based on the mass of NiHCF. At both 1 C and C/2 rates, the battery

was heated up to 55 ^{o}C and charged to 640.0 mV. Then it was cooled down to 15 ^{o}C which increased the open circuit voltage (OCV) to 660.1 mV for 1 C and 661.6 mV for C/2. Next, the cell was discharged to 485 mV at 15^{o}C and then heated up to 55 ^{o}C again. The electricity produced in one cycle (W) normalized to the mass of NiHCF can be written as

$$W = Q_{dis}\bar{V}_{dis} - Q_{ch}\bar{V}_{ch} = Q_{dis}(\bar{V}_{dis} - \bar{V}_{ch}/CE) \qquad (4)$$

where Q and $\bar{V}$ are the specific capacity normalized to the mass of NiHCF and average full cell voltage, respectively. The subscript *dis* and *ch* indicate discharge and charge, respectively. CE is the coulombic efficiency, which is defined as Q_{dis}/Q_{ch}. From equation (4), we can see that in addition to large specific discharge capacity and voltage gap between discharge and charge, high coulombic efficiency is also important to achieve high energy output and conversion efficiency. $\bar{V}_{dis} - \bar{V}_{ch}$ and $\bar{V}_{dis} - \bar{V}_{ch}/CE$ are defined as the apparent and effective voltage gap, respectively, as the latter one directly determines the energy difference between discharge and charge.

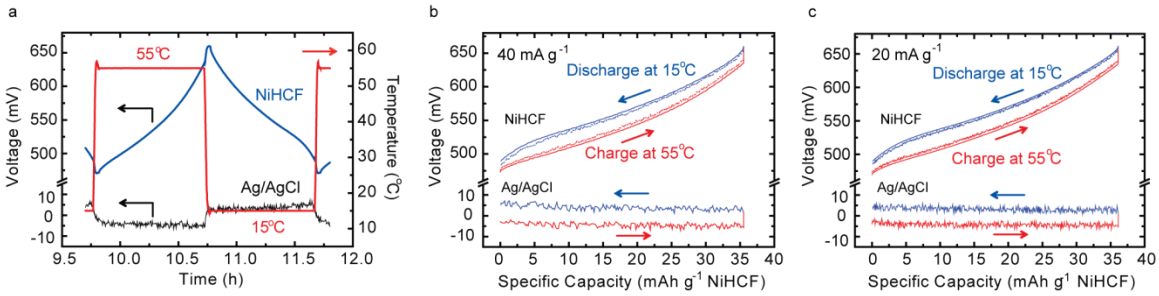

Figure 3. Thermal cycle of a NiHCF/Ag/AgCl/3M KCl full cell. (a) A voltage vs. time plot showing the charge and discharge curves of both NiHCF cathode (blue) and Ag/AgCl anode (black). The reference electrode is the Ag/AgCl electrode in the pouch. The current rate is 40 mA g^{-1}. (b) and (c) The voltage vs. specific capacity plot at (b) 40 and (c) 20 mA g^{-1}. The dashed lines at the inner side of voltage profiles of NiHCF in (b) and (c) are the full cell voltage. Magnified

voltage profiles of electrodes and full cells are shown in Figure S5. All currents are based on the mass of NiHCF.

At 1 C rate (Figure 3b), the average discharge voltages of NiHCF and Ag/AgCl were 566.27 and 4.37 mV, respectively, and the capacity is 35.4 mAh g^{-1} based on the mass of NiHCF. The average charge voltages of NiHCF and Ag/AgCl were 542.42 and -3.93 mV, respectively, and the capacity is 35.5 mAh g^{-1}. As a result, the apparent and effective voltage gaps are 15.8 and 14.2 mV, respectively. The total specific discharge and charge energy are 19.90 mWh g^{-1} and 19.40 mWh g^{-1}, respectively; thus 0.50 mWh g^{-1} of heat energy was converted to electricity. Based on equation (2) and procedures discussed in our previous publication[9], The heat-to-electricity conversion efficiency (η) was calculated as

$$\eta = \frac{W}{T_H \Delta S + Q_{HR}} = \frac{W_{discharge} - W_{charge}}{|\alpha| T_H Q_c + (1 - \eta_{HR}) C_p \Delta T} \qquad (5)$$

where W is the difference between discharge and charge energy in a cycle. Q_c is the discharge capacity at T_H, η_{HR} is the heat recuperation efficiency, and 50-70% are reasonable[9]. Other parameters are defined as same as those in equation (2). As W is calculated based on experimentally measured voltage profiles (Fig. 3b and c), changes in concentration of K^+ and Cl^- are taken into account. In the process described above, $Q_H =$ 8.617 mWh g^{-1} with α of -0.74 mV K^{-1}. The total heat capacity of electrolytes and electrodes are 2.84 J g^{-1} K^{-1} and $C_p \Delta T$= 31.6 mWh g^{-1} for cycle between 15 and 55 ^oC. Based on these values, η reaches 1.3%, 2.1% and 2.8% for η_{HR} of 0%, 50% and 70%. The calculation above is also presented as Table 1 and the details are described in the supporting information.

Similarly, the voltage curves at C/2 rate (20 mA g^{-1}) tested in the same voltage range are plotted as Figure 3c. For the full cell, the average discharge voltage increases to 565.7 mV and the average charge voltage decreases to 545.8 mV, as lower current leads to smaller overpotential. The specific capacity also increases to 36.0 and 36.1 mAh g^{-1} for discharge and charge, respectively. Consequently the discharge and charge energy are 20.35 mWh g^{-1} and 19.71 mWh g^{-1}, respectively. The energy converted to electricity reaches 0.65 mWh g^{-1}, 29% higher than that at 1 C rate, and the corresponding η are 1.6%, 2.6% and 3.5% for η_{HR} of 0%, 50% and 70%.

Table 1. Calculation of conversion efficiency at different current rate*

Current rate	$\bar{V}_{dis}$ (mV)	$\bar{V}_{ch}$ (mV)	Q_{dis} (mAh g^{-1})	CE (%)	W (mWh g^{-1})	Q_H (mWh g^{-1})	$C_p\Delta T$ (mWh g^{-1})	Conversion efficiency at different η_{HR}		
								0%	50%	70%
1 C	561.9	546.4	35.4	99.72	0.50	8.62	31.6	1.3	2.1	2.8
C/2	565.7	545.8	36.0	99.72	0.65	8.76	32.1	1.6	2.6	3.5

* All symbols are the same as those in equation (2), (4) and (5)

For long term operation, cycle life of TREC is crucial. The specific capacity, coulombic efficiency, average charge/discharge voltage, and thermal-to-electricity efficiency are plotted against cycle number as Figure 4a, b and c in sequence. The cell was cycled at 1 C rate for the first 35 cycles, then at C/2 for 50 cycles. The capacity fading rate is on average 0.10% and 0.18% per cycle at 1 C and C/2, respectively. The higher capacity fading at C/2 is likely due to a longer operation time at 55 ^{o}C. The Coulombic efficiency is 99.2% at the beginning, but quickly increases to ~ 99.5-99.7% after 5 cycles. The average charge/discharge voltage shows a steady increasing trend of ~0.1 mV per cycle (Figure 4b). The origin of this is not yet clear. Figure 4b also shows

that the apparent voltage gap between charge and discharge ($\bar{V}_{dis} - \bar{V}_{ch}$) is about 4 mV higher at C/2 compared to 1 C rate, as a result of lower overpotential at smaller current. Moreover, the effective voltage gap ($\bar{V}_{dis} - \bar{V}_{ch}/CE$) is obviously lower than the apparent voltage gap ($\bar{V}_{dis} - \bar{V}_{ch}$) due to non-100% Coulombic efficiency. The difference is ~5 mV at the beginning and decreases to ~2 mV as the Coulombic efficiency gradually increases and stabilizes around 99.7%. The absolute conversion efficiency (η) is a synergistic result of the three factors above based on equation (4) (Figure 4c). At 70% heat recuperation, η is 2.2% in the first cycle due to low Coulombic efficiency, and gradually increases to 2.9% after 30 cycles. The following cycles at C/2 shows η of 3.5% at the beginning and it decreases slowly to 2.9% after 50 cycles. This is because CE is steady in this part and the major fading factor is the decreasing capacity and apparent voltage gap. The fading rate is much smaller than our previous work[9] as evaporation is fully eliminated by employing pouch cell configuration. In addition, it should be noticed that AgCl has a noticeable solubility in KCl solution, which is ~1 mM in 3 M KCl solution at room temperature[21]. This may lead to degradation of the anode and accumulation of Ag at cathode. The effect of soluble Ag ions on long-term cycling needs further investigation.

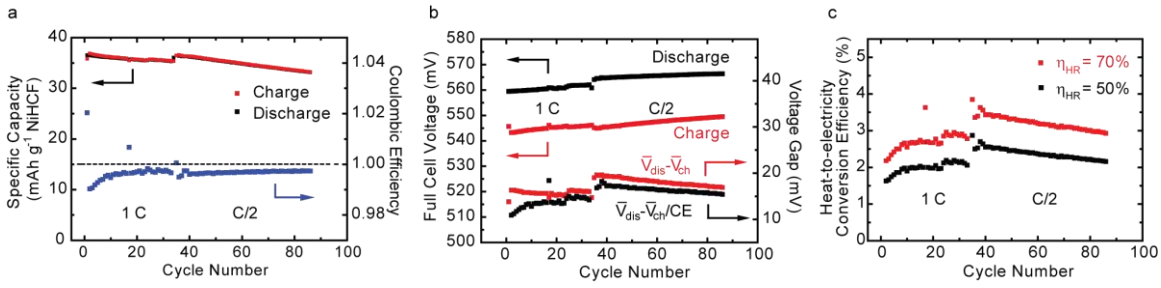

Figure 4. Cycling performance of NiHCF/Ag/AgCl system for TREC. a) Discharge/charge capacity and Coulombic efficiency vs. cycle life. b) Average full cell charge/discharge voltage and their difference vs. cycle life. c) The thermal-to-electricity conversion efficiency vs. cycle life.

As thermoelectrics is a major research focus for waste heat harvesting[4, 7], it would be useful to compare the current work and thermoelectrics (TE). We would like to first point out that there are many differences between these two approaches (TE vs. TREC). TE is based on transport characteristics, such as thermal and electrical conductivity, while TREC relies on thermodynamic properties, such as heat capacity and temperature coefficient[9]. Given the low temperature differential for low-grade heat, isothermal operation may be easier than temperature gradient based technologies. However, currently the typical cycle time of TREC is in the order of one hour, leading to much lower power (~1 W g^{-1}) than TE, as ionic transport and electrochemical reaction is slower than electronic transport. TREC also faces challenges in long term operation, which may requires thousands of cycles at elevated temperature. With these differences in mind, a conversion of the efficiencies above to equivalent ZT values helps evaluate the performance of TREC. At a heat recuperation efficiency of 70%, efficiency achieved at 1C and C/2 are 2.8 and 3.5% for temperature cycle between 15 and 55 ^{o}C. A TE device needs to reach ZT of 1.4 and 2.1 to achieve the same efficiency for the same high and low temperatures. If heat recuperation efficiency of 50% is assumed, the corresponding effective ZTs are 0.94 and 1.3 for efficiencies at 1C (2.1%) and C/2 (2.6%), respectively. In contrast, state-of-the-art TE materials have a ZT of 1-1.5 for temperature below 100 ^{o}C[7, 22]. Again, we want to emphasize that there are remarkable differences between the two approaches and readers should keep this in mind to understand the strengths and limits of both approaches.

A possible concern of the NiHCF/AgCl/Ag system is the cost of Ag. An estimation based on the price of Ag and Nafion ion-selective membrane shows that even with high mass loading of Ag (5 mg cm^{-2}), the cost is still less than 20% of Nafion membranes. When power density is considered, the cost of Ag electrode per watt is slightly less than half of membrane used in CuHCF//Cu^{2+}/Cu system reported before[9] (see supporting information for details). Searching for inexpensive electrodes to replace Ag can further reduce the cost.

In summary, a membrane-free electrochemical system with nickel hexacyanoferrate (NiHCF, $KNi^{II}Fe^{III}(CN)_6$) cathode and Ag/AgCl anode is demonstrated to convert low-grade heat tot electricity. As ions involved in each electrode do not interfere with the opposite electrode, expensive ion-selective membranes are not needed in this system. The system shows a thermo-to-electricity conversion efficiency of 3.5% under 70% heat recuperation when it is cycled between 15 and 55 ^{o}C. The system also shows adequate cycle life compared to previous results. We believe that further optimization and searching for new systems will lead to new development and possibly practical deployment of TREC.

Acknowledgments

The authors acknowledge support from Solid-State Solar-Thermal Energy Conversion Center (S^3TEC), an Energy Frontier Research Center funded by the U.S. Department of Energy, Office of Science, Office of Basic Energy Sciences under Award Number: DE-SC0001299/DE-FG02-09ER46577 (Y.Y., J.L., H.G., G.C. for experiments and analysis), AFOSR (G.C. for experimental system), and by DOE EERE Award No. DE-EE0005806. Y.C. acknowledges the support by the U.S. Department of Energy, Office of Basic Energy Sciences, Division of Materials Sciences and Engineering under

Contract No. DE-AC02-76SF00515 through the SLAC National Accelerator Laboratory LDRD project. H.-W.L. acknowledges the support from Basic Science Research Program through the National Research Foundation of Korea (NRF) funded by the Ministry of Education, Science and Technology under Contract No. 2012038593.

References:

1. Chu, S.; Majumdar, A. *Nature* **2012,** 488, (7411), 294-303.

2. Gur, I.; Sawyer, K.; Prasher, R. *Science* **2012,** 335, (6075), 1454-1455.

3. Rattner, A. S.; Garimella, S. *Energy* **2011,** 36, (10), 6172-6183.

4. Zebarjadi, M.; Esfarjani, K.; Dresselhaus, M. S.; Ren, Z. F.; Chen, G. *Energy & Environmental Science* **2012,** 5, (1), 5147-5162.

5. Biswas, K.; He, J.; Blum, I. D.; Wu, C.-I.; Hogan, T. P.; Seidman, D. N.; Dravid, V. P.; Kanatzidis, M. G. *Nature* **2012,** 489, (7416), 414-418.

6. Snyder, G. J.; Toberer, E. S. *Nature Materials* **2008,** 7, (2), 105-114.

7. Poudel, B.; Hao, Q.; Ma, Y.; Lan, Y.; Minnich, A.; Yu, B.; Yan, X.; Wang, D.; Muto, A.; Vashaee, D.; Chen, X.; Liu, J.; Dresselhaus, M. S.; Chen, G.; Ren, Z. *Science* **2008,** 320, (5876), 634-638.

8. Tchanche, B. F.; Lambrinos, G.; Frangoudakis, A.; Papadakis, G. *Renewable & Sustainable Energy Reviews* **2011,** 15, (8), 3963-3979.

9. Seok Woo Lee, Y. Y., Hyun-Wook Lee, Hadi Ghasemi, Daniel Kraemer, Gang Chen, Yi Cui. *Nature Communications* **2014,** 5, 3942.

10. HELENA L. CHUM, R. A. O. *Review of thermally regenerative electrochemical systems*; NTIS, order No. DE81029624; Solar Energy Research Institute: 1981.

11. Anderson, L. B.; Greenber.Sa; Adams, G. B. *Advances in Chemistry Series* **1967**, (64), 213-276.

12. Debethune, A. J.; Licht, T. S.; Swendeman, N. *Journal of the Electrochemical Society* **1959,** 106, (7), 616-625.

13. Quickenden, T. I.; Mua, Y. *Journal of the Electrochemical Society* **1995,** 142, (11), 3985-3994.

14. Kuzminskii, Y. V.; Zasukha, V. A.; Kuzminskaya, G. Y. *Journal of Power Sources* **1994,** 52, (2), 231-242.

15. Hesson, J. C.; Shimotake, H., Thermodynamics and Thermal Efficiencies of Thermally Regenerative Bimetallic and Hydride EMF Cell Systems. In *Regenerative EMF Cells*, Crouthamel, C. E.; Recht, H. L., Eds. American Chemical Society: Washington, D.C., 1967; Vol. 64, pp 82-104.

16. Chum, H. L.; Osteryoung, R. A. *Review on thermally regenerative electrochemical system*; Solar Energy Research Institute: Golden, CO, 1981.

17. Wessells, C. D.; Peddada, S. V.; Huggins, R. A.; Cui, Y. *Nano Letters* **2011,** 11, (12), 5421-5425.

18. Lu, Y.; Wang, L.; Cheng, J.; Goodenough, J. B. *Chemical Communications* **2012,** 48, (52), 6544-6546.

19. Birss, V. I.; Smith, C. K. *Electrochimica Acta* **1987,** 32, (2), 259-268.

20. Wang, R. Y.; Wessells, C. D.; Huggins, R. A.; Cui, Y. *Nano Letters* **2013,** 13, (11), 5748-5752.

21. Forbes, G. S. *Journal of the American Chemical Society* **1911,** 33, 1937-1946.

22. Liu, W.-S.; Zhang, Q.; Lan, Y.; Chen, S.; Yan, X.; Zhang, Q.; Wang, H.; Wang, D.; Chen, G.; Ren, Z. *Advanced Energy Materials* **2011,** 1, (4), 577-587.

Supporting Information for

A Membrane-free Battery for Harvesting Low-grade Thermal Energy

Yuan Yang[1], James Loomis[1], Hadi Ghasemi[1], Seok Woo Lee[2], Jenny Wang[1], Yi Cui[2,3a] and Gang Chen[1a]

[1]Department of Mechanical Engineering, Massachusetts Institute of Technology, Cambridge, MA, 02139, USA. [2]Department of Materials Science and Engineering, Stanford University, Stanford, CA, 94305, USA. [3]Stanford Institute for Materials and Energy Sciences, SLAC National Accelerator Laboratory, 2575 Sand Hill Road, Menlo Park, CA 94025, USA.

[a]To whom correspondence should be addressed. Email: gchen2@mit.edu yicui@stanford.edu

Materials Preparation

All chemicals for synthesis of nickel hexacyanoferrate (NiHCF) were purchased from Sigma Aldrich. To synthesize NiHCF, 40 mL of 50 mM $Ni(NO_3)_2$ was dropped in 40 mL of 25 mM $K_3Fe(CN)_6$ under strong stirring at 50 ^oC. The speed is about one drop per second. The precipitation was centrifuged and dried at 70 ^oC overnight.[1, 2] The TEM image is shown as Figure S1. The NiHCF electrode was prepared by mixing 70 wt% NiHCF nanoparticles, 20 wt% Super P carbon black, and 10% polyvinylidene fluoride (PVdF, Kynar) in N-Methyl-2-pyrrolidone (NMP) and drop casting onto carbon cloth disc electrode (Fuel Cell Store) at 90 ^oC. The carbon cloth disc had a diameter of 1 cm and the mass loading is about 3 mg NiHCF cm^{-2}. Ag foil with 25 μm thickness and size

of 2 cm by 2 cm served as the negative electrode. Glass fiber filter (Whatman) was used as the separator.

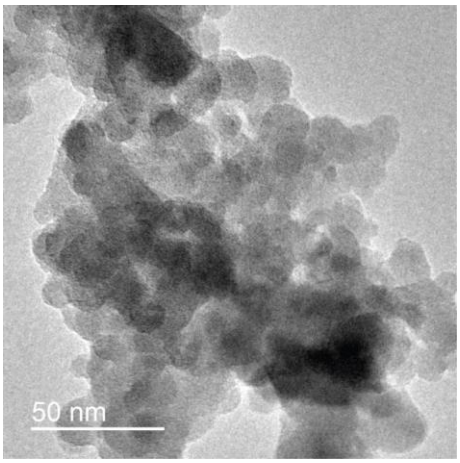

Figure S1. The TEM image of as-prepared NiHCF. The typical particle size is 20-30 nm.

Electrochemistry.

All electrochemical measurements were performed using the pouch cell configuration as illustrated in Figure S2a and S2b. Pt and Ag foils were used as current collectors for cathode and anode, respectively. The Ag/AgCl reference electrode was made by precharging a silver rod in 1 M KCl solution. Then the Ag film anode was partially charged by the AgCl reference electrode inside the pouch cell to make a Ag/AgCl anode with a high porous surface area[3]. The specific process was to charge the Ag film to 1 mAh and then discharge back by 0.5 mAh. Then the *in-situ* formed Ag/AgCl film electrode acts as the anode. The typical amount of electrolyte is 500 μl. The typical thickness of the cell is 1-1.5 mm. All electrochemical measurements were done with a Bio-Logic VSP300 tester. The temperature cycling was done with a home-made thermoelectric-based temperature cycler, which is described in the following section.

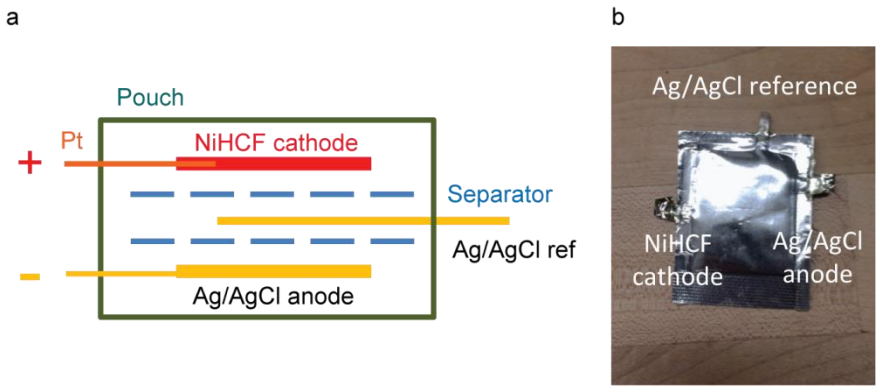

Figure S2. The pouch cell configuration used in electrochemical test. (a) A schematic of pouch cell used. (b) A camera image of a fabricated pouch.

Temperature Cycling

Heating and cooling of the pouch cell was controlled by thermoelectric plates. A 2 mm thick aluminum sheet was placed on each side of the pouch to ensure uniform heating and cooling. Thermopaste (Omega) was applied on all interfaces to ensure good thermal contact. Temperature were measured by thermocouples on both side of the pouch and controlled by labview programs, as illustrated in Figure S3a. The setup and power supply are shown in Figure S3b and c, respectively.

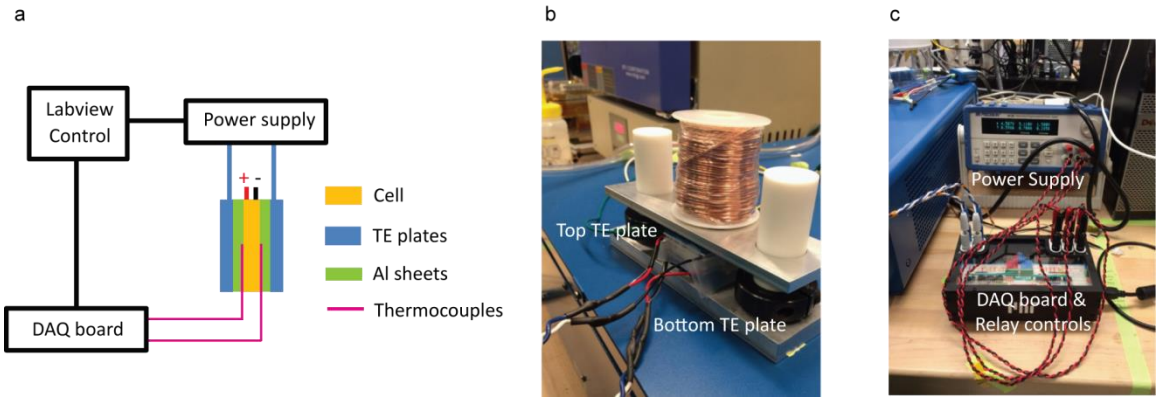

Figure S3. The home-made thermal cycler for temperature coefficient measurement and thermal cycling. (a) The structure of the system. The cell and TE plates are not drawn to scale. (b) A camera image of the setup. (c) The DAQ board and power supply used in the system.

For the temperature coefficient measurement, the temperature was changed in the sequence of 55, 15, 45, 25, 35 and 15 ^{o}C. Figure S4a shows a typical measurement with the electrode potential of both NiHCF and Ag/AgCl electrodes presented. For thermal cycling between 55 and 15 ^{o}C, the current acquired by the EC-lab software for VMP3 tester was monitored. Once a step (charge or discharge) was finished as current became zero, the temperature is switched accordingly. A real-time plot of voltage and temperature is shown as Fig. 3a in the main text.

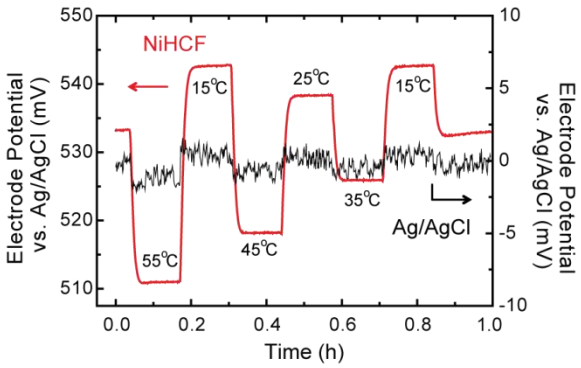

Figure S4. Real time measurement of temperature coefficient. The temperature was set 55, 15, 45, 25, 35 and 15 ^{o}C in sequence. Each step lasted for 8 minute. The pouch cell configuration described above was used and the potential was measured using a reference of Ag/AgCl electrode exposed to the same electrolyte in the pouch.

Magnified Voltage Profile

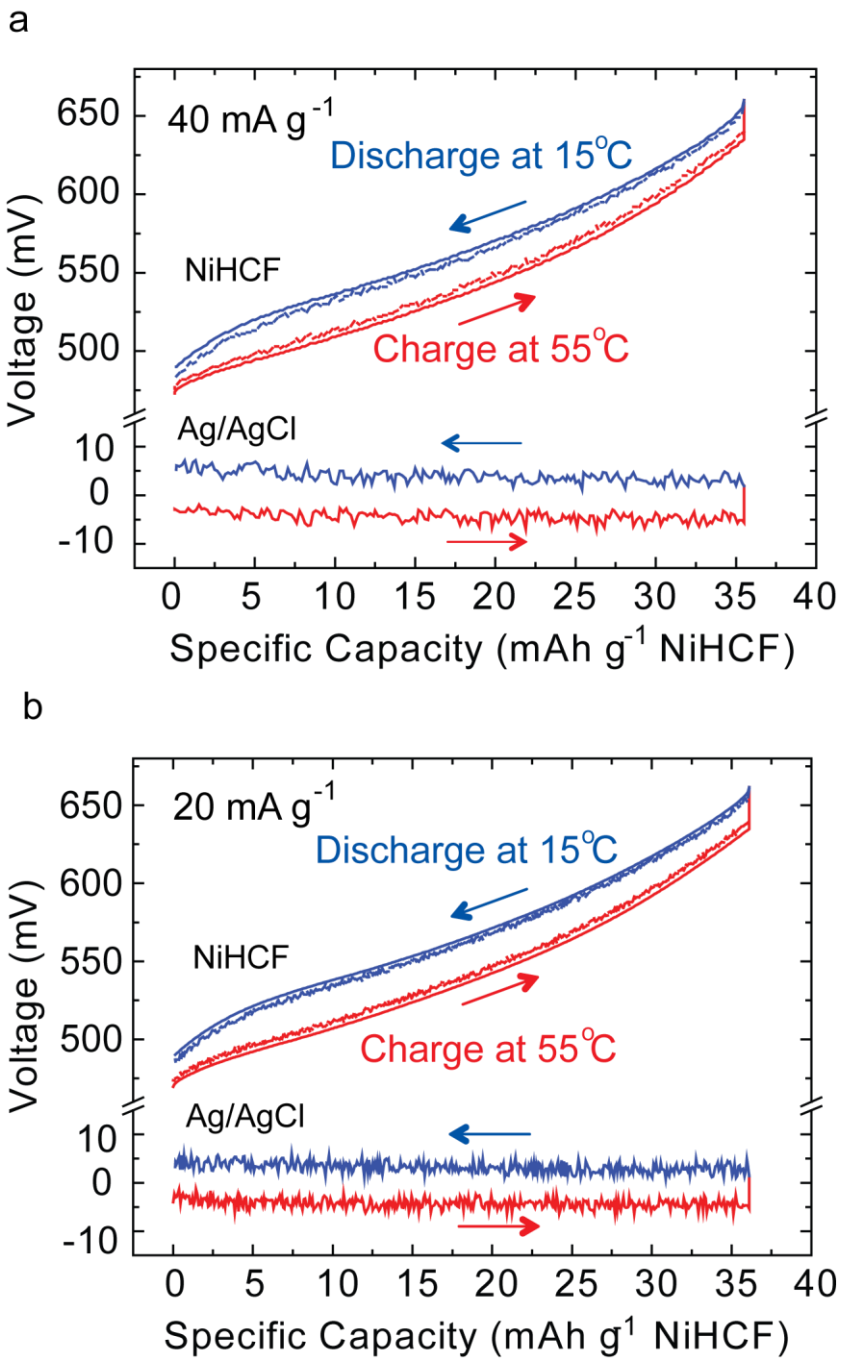

Figure S5. a) and (b) The voltage vs. specific capacity plot at (b) 40 and (c) 20 mA g^{-1}. The dashed and rough lines at the inner side of the voltage profile of NiHCF are those of full cells.

Efficiency Calculation

The efficiency was calculated based on equation (4) in the main text, which is copied here:

$$\eta = \frac{W}{Q_H + Q_{HR}} = \frac{W_{discharge} - W_{charge}}{|\alpha| T_H Q_c + (1 - \eta_{HR}) C_p \Delta T}$$

where W is the difference between discharge and charge energy in a cycle. Q_H is the heat absorbed at T_H (55 ^oC). Q_{HR} is the extra energy needed to heat the cell up. Q_c is the discharge capacity at T_H, C_p is the heat capacity of the cell. η_{HR} is the heat recuperation efficiency, indicating how much energy rejected in the cooling process can be reused for the next heating process, and 50-70% are reasonable as demonstrated in our previous work.[4]

The cycle described in Figure 3b is selected for an example efficiency calculation. To simplify the calculations, all values were normalized to the mass of NiHCF. W is calculated based on the full cell voltage curves (dashed line in Figure 3b) as $W_{discharge} - W_{charge}$. Its value is 0.50 mWh g^{-1} based on the mass of NiHCF.

$$Q_H = |\alpha| T_H Q_c = 0.74mV \times 328K \times 35.5\, mAh\, g^{-1} = 8.62 \text{ mWh } g^{-1}$$

In calculating C_p, the specific heat of NiHCF, Ag and 3 M KCl electrolyte is considered. The specific heat of NiHCF is 1.1 J g^{-1} based on DSC measurement. For 1 gram of NiHCF electrode, the amount of 3 M KCl electrolyte needed is 35.5 mAh / (96485 C mol^{-1}*3 mol L^{-1}) = 0.442 mL. The specific heat of 3 M KCl is 3.1 J g^{-1} K^{-1} based on DSC measurement and its density is 1.22 g mL^{-1}. The amount of Ag needed is 35.5 mAh / (96.485 C mol^{-1} / 108 g mol^{-1}) = 0.133 g. The specific heat of Ag is 0.24 J g^{-1} K^{-1}. So the heat capacity based on the mass of NiHCF is 1.1 + 3.1*1.23*0.442 + 0.133*0.24 = 2.82 J g^{-1} K^{-1}. As ΔT = 40 K, $C_p \Delta T$ = 112.8 J g^{-1} = 31.3 mWh g^{-1}.

Consequently the heat-to-electricity conversion efficiency with η_{HR} = 50% is

$$\eta = \frac{0.50}{8.62+31.3\times(1-0.5)} = 2.1\%.$$

Similarly, to estimate the optimized concentration of KCl electrolyte, the efficiency at different [KCl] was calculated and listed in Table S1. The temperature coefficients at different [KCl] were obtained as the value at 50% state of charge in Figure 2c. The voltage gap was the average difference between discharge and charge voltage after taking accounting for overpotential. 12 mV was used for the overpotential based on data at 1 C and C/2 rates (Figure 3b and c). The heat capacities of KCl electrolyte at all concentrations were assumed to 4.0 J cm^{-3} K^{-1}. The heat capacities of NiHCF, Ag and the KCl electrolyte were taken into account. From table S1, 3 M is the optimal concentration.

Table S1. Estimation of heat-to-electricity efficiency at different [KCl]

[KCl] (M)	temperature coefficient α (mV K^{-1})	αΔT (mV)	voltage gap (mV)	W (mWh g^{-1})	Q_H (mWh g^{-1})	$C_p\Delta T$ (mWh g^{-1})	Efficiency with h_{HR} =50% (%)	Efficiency with h_{HR} =70% (%)
1	-1.04	41.6	29.6	1.07	12.3	72.3	2.20	3.14
2	-0.80	32	20	0.72	9.45	42.5	2.35	3.25
3	-0.75	30	18	0.65	8.86	32.5	2.58	3.48
4	-0.63	25.2	13.2	0.48	7.44	27.5	2.24	3.03

Cost analysis

The cost of ion-selective membrane used in our previous work is ~\$200 m^{-2}. For Ag, the current mass loading requires 0.7 mg Ag cm^{-2}. Suppose that 5 mg cm^{-2} is needed in a real cell due to increased capacity per area, then 50 gram is needed per square meter, which costs about \$35 m^{-2} (\$700 kg^{-1}), much less than the ion-selective membrane. For cost per watt, if the internal resistance is assumed to be the same for NiHCF/AgCl and CuHCF//

Cu^{2+}/Cu systems, the power generation scales with α^2 (-0.74 mV/K for NiHCF/AgCl and -1.2 mV/K for CuHCF// Cu^{2+}/Cu) when temperatures of hot and cold sources are the same. The cost of Ag per watt would be slightly less than half of the cost of ion-selective membrane. Searching for new materials with low cost and developing cheap ion-selective membrane are two important directions for future research.

Reference:

1. Wessells, C. D.; Peddada, S. V.; Huggins, R. A.; Cui, Y. *Nano Letters* **2011,** 11, (12), 5421-5425.
2. Lu, Y.; Wang, L.; Cheng, J.; Goodenough, J. B. *Chemical Communications* **2012,** 48, (52), 6544-6546.
3. Jin, X. B.; Lu, J. T.; Xia, Y.; Liu, P. F.; Tong, H. *Journal of Power Sources* **2001,** 102, (1-2), 124-129.
4. Seok Woo Lee, Y. Y., Hyun-Wook Lee, Hadi Ghasemi, Daniel Kraemer, Gang Chen, Yi Cui. *Nature Communications* **2013,** 5, 3942.